Gain-of-Function *MN1* Truncation Variants Cause a Recognizable Syndrome with Craniofacial and Brain Abnormalities

Noriko Miyake,[1,*] Hidehisa Takahashi,[2] Kazuyuki Nakamura,[3] Bertrand Isidor,[4] Yoko Hiraki,[5] Eriko Koshimizu,[1] Masaaki Shiina,[6] Kazunori Sasaki,[2] Hidefumi Suzuki,[2] Ryota Abe,[2] Yayoi Kimura,[7] Tomoko Akiyama,[7] Shin-ichi Tomizawa,[8] Tomonori Hirose,[2] Kohei Hamanaka,[1] Satoko Miyatake,[1,9] Satomi Mitsuhashi,[1] Takeshi Mizuguchi,[1] Atsushi Takata,[1] Kazuyuki Obo,[8] Mitsuhiro Kato,[3,10] Kazuhiro Ogata,[6] and Naomichi Matsumoto[1,*]

MN1 was originally identified as a tumor-suppressor gene. Knockout mouse studies have suggested that *Mn1* is associated with craniofacial development. However, no *MN1*-related phenotypes have been established in humans. Here, we report on three individuals who have *de novo MN1* variants that lead to a protein lacking the carboxyl (C) terminus and who presented with severe developmental delay, craniofacial abnormalities with specific facial features, and structural abnormalities in the brain. An *in vitro* study revealed that the deletion of the C-terminal region led to increased protein stability, an inhibitory effect on cell proliferation, and enhanced MN1 aggregation in nuclei compared to what occurred in the wild type, suggesting that a gain-of-function mechanism is involved in this disease. Considering that C-terminal deletion increases the fraction of intrinsically disordered regions of MN1, it is possible that altered phase separation could be involved in the mechanism underlying the disease. Our data indicate that MN1 participates in transcriptional regulation of target genes through interaction with the transcription factors PBX1, PKNOX1, and ZBTB24 and that mutant MN1 impairs the binding with ZBTB24 and RING1, which is an E3 ubiquitin ligase. On the basis of our findings, we propose the model that C-terminal deletion interferes with MN1's interaction molecules related to the ubiquitin-mediated proteasome pathway, including RING1, and increases the amount of the mutant protein; this increase leads to the dysregulation of MN1 target genes by inhibiting rapid MN1 protein turnover.

Introduction

MN1 (MN1 proto-oncogene, transcriptional regulator, MIM: 156100, GenBank: NM_002430.3) at 22q12.1 consists of two exons encoding 1,320 amino acid residues in humans. It was first reported as a disrupted gene of t(4;22) in meningioma or t(12;22) in myeloproliferative disorder.[1,2] Thus, *MN1* was thought to be a tumor-suppressor gene associated with the inhibition of cell proliferation. Conversely, *MN1* has also been described as an oncogene because high *MN1* expression is associated with the poor prognosis of acute myeloid leukemia.[3]

As a transcription cofactor, MN1 increases its transactivation capacity in synergy with all-*trans* retinoic acid (ATRA) and coactivators EP300 (formerly P300) and RAC3 in a dose-dependent manner.[4] MN1 recognizes a "CACCC" sequence, as well as the DR1 (AGGT CAAAGGTCA) and DR5 (AGTTCAGATCAAGGTCA) sequences,[4] which are classical consensus sequences for retinoic acid receptors.[5,6] However, MN1 cannot bind directly to these sequences, and other proteins are needed to allow MN1 to bind DR1 and DR5.[4] Molecules directly binding MN1, and the mechanisms of MN1-induced inhibition in cell proliferation, have not yet been elucidated.

MN1 has been implicated in brain and craniofacial development in mice and humans.[7–9] In mice, *Mn1* is strongly expressed in the midbrain, hindbrain, and craniofacial mesenchyme at embryonic day 9.5 (E9.5) and in all the prominences of the developing face by E10.5.[9] *Mn1* exhibits notable differential expression along the anteroposterior axis of the developing second plate during palatal outgrowth.[9] Homozygous *Mn1*-knockout mice die at or soon after birth because of a cleft palate, and preterm (E15.5 to E17.5) null mice undergo abnormal skull bone development.[10] Heterozygous knockout mice display a less severe phenotype, involving hypoplastic membranous bone and incomplete penetrance of the cleft palate.[10] In humans, at least nine individuals with a heterozygous deletion involving *MN1* have been reported, and all have orofacial features, including a cleft palate.[7,11,12] However, because other genes were also deleted in these individuals, it remains unknown whether *MN1* deletion alone affects human development.

Here, we report on three individuals with a recognizable syndrome involving characteristic craniofacial and brain abnormalities caused by gain-of-function *MN1* variants that produce C-terminally truncated proteins. In addition, we shed light on a characteristic property of MN1: it

[1]Department of Human Genetics, Yokohama City University Graduate School of Medicine, Yokohama 236-0004, Japan; [2]Department of Molecular Biology, Yokohama City University Graduate School of Medicine, Yokohama 236-0004, Japan; [3]Department of Pediatrics, Yamagata University Faculty of Medicine, Yamagata 990-9585, Japan; [4]Service de Génétique Médicale, Centre Hospitalier Universitaire de Nantes, 44093 Nantes, France; [5]Hiroshima Municipal Center for Child Health and Development, Hiroshima 732-0052, Japan; [6]Department of Biochemistry, Yokohama City University Graduate School of Medicine, Yokohama, 236-0004, Japan; [7]Advanced Medical Research Center, Yokohama City University, Yokohama 236-0004, Japan; [8]Department of Histology and Cell Biology, Yokohama City University School of Medicine, Yokohama 236-0004, Japan; [9]Clinical Genetics Department, Yokohama City University Hospital, Yokohama, 236-0004, Japan; [10]Department of Pediatrics, Showa University School of Medicine, Tokyo 142-8666, Japan
*Correspondence: nmiyake@yokohama-cu.ac.jp (N.Mi.), naomat@yokohama-cu.ac.jp (N.Ma.)
https://doi.org/10.1016/j.ajhg.2019.11.011.

contains an intrinsically disordered region (IDR), possibly related to phase separation in cells. The identified mutants all increase the proportion of MN1 that is intrinsically disordered.

Methods

DNA Preparation and Genetic Analysis

We collected samples after obtaining written informed consent from study participants. DNA was extracted from human peripheral leukocytes. Whole-exome sequencing (WES) was performed as previously reported.[13] The candidate variants were validated by Sanger sequencing. This study was approved by the institutional review board of the Yamagata University Faculty of Medicine and the Yokohama City University School of Medicine.

Cell Culture

HEK293T, HeLa, MG63, Plat-E, and HeLa S3 cells stably expressing mCAT (mCAT-HaLa) cells were grown in DMEM-GlutaMAX (Thermo Fisher) with 10% heat-inactivated fetal bovine serum (FBS, Sigma-Aldrich,) and penicillin-streptomycin (Thermo Fisher) at 37°C with 5% CO_2 concentration. A human lymphoblastoid cell line was established from peripheral blood by SRL and maintained with RPMI 1641 media (Thermo Fisher) with 10% heat-inactivated FBS and antibiotic antimycotic solution (Sigma-Aldrich) at 37°C with 5% CO_2 concentration.

MN1 Subcellular Localization in HeLa Cells

An N-terminal GFP-fused human *MN1* expression vector was created by incorporating the *MN1* (GenBank: NM_002430.3) open-reading frame (ORF) into DEST53 via the Gateway cloning system (Thermo Fisher). The human *MN1* ORF was amplified with a human cDNA library purchased from Clontech. The mutant was created by a KOD-plus-Mutagenesis Kit (TOYOBO). We transfected 500 ng of each construct into HeLa cells by using ViaFect Transfection Reagent (Promega). After 48 h of transfection, the cells were fixed with 2% paraformaldehyde, washed with 1× PBS, and mounted onto slides with a mounting medium and DAPI (Vector Laboratories).

Quantification of MN1 Aggregation

Wild-type or mutant GFP-tagged MN1 was transiently overexpressed in HeLa cells. The cells were washed with 1× PBS 48 h after transfection and fixed with 2% paraformaldehyde in 1× PBS for 15 min at room temperature. After being washed three times with 1× PBS, the coverslips were mounted with antifade solution containing DAPI (Vector Laboratories). Confocal microscopy images of the HeLa cells were captured with ApoTome and ZEN black (Zeiss). Ten images of each construct were captured (63× objective lens, 0.5× zoom with oil-immersion lens) and analyzed with ImageJ and a custom R program. The MN1 aggregates within the cells were selected, and the area and mean intensity of each aggregate were measured.

Protein Stability Assay

We created N-terminal V5-tagged human *MN1* expression vectors by using the Gateway cloning system (Thermo Fisher) to incorporate the *MN1* ORF into pcDNA3.1/nV5-DEST (Thermo Fisher). The mutant was created with the KOD-plus-Mutagenesis Kit (TOYOBO). N-terminal V5-tagged wild-type and mutant MN1 constructs were transiently transfected into HEK293T cells via X-tremeGENE 9 DNA transfection reagent (Roche). 48 h after transfection, cells were treated with cycloheximide (CHX) at 80 μg/mL both with and without MG132 (25 μM) for 6 h (cells not treated with CHX and MG132 were assigned a treatment value of 0 h). Cells were collected with trypsin, lysed with lysis buffer (25 mM Tris-HCl [pH 7.5], 100 mM NaCl, 2 mM EDTA, and 0.5% Triton X-100) with AEBSF protease inhibitor (Thermo Fisher) and Benzonase Nuclease (Sigma-Aldrich). The same amounts of whole fraction for each sample were loaded on 4%–12% Bis-Tris gels for immunoblotting. Anti-V5 mouse monoclonal antibodies (Catalogue #R960-25, 1:5000, Thermo Fisher) and anti-β-actin mouse monoclonal antibodies (Catalogue #ab6276, 1:5000, Abcam) were incubated in 5% non-fat milk in PBST (1× phosphate-buffered saline and 0.1% Tween), and horseradish peroxidate (HRP) anti-mouse IgG antibodies (catalogue #115-035-003, 1:10,000, Jackson ImmunoResearch) were used as the secondary antibodies. Protein signals were detected with SuperSignal West Dura Extended Duration Substrate (Thermo Fisher) by the ChemiDoc Touch Imaging System (Bio-Rad). The signal intensity was measured with Image Lab software (Bio-Rad). The V5-tagged MN1 levels were normalized with β-actin. The MN1 protein of cells with no treatment was set to be 100% for each construct's transfection. Statistical analysis was performed with R 3.6.1 by Welch's test between no treatment and CHX and by t test between CHX and CHX with MG132.

Luciferase Reporter Assay

The wild-type and three mutant versions of the *MN1* ORF were incorporated into the pBIND vector via the In-Fusion HD Cloning kit (Takara Bio). pBIND-VP16 was used for positive control of transcriptional activity. In addition to each pBIND-MN1 construct, pGL4.31 and PRL-tk were co-transfected into HEK293T cells with X-tremeGENE 9 (Roche). Triplicate samples for each construct were measured in three independent experiments. 48 h after transfection, cells were collected and analyzed with the Dual-Luciferase Reporter Assay system (Promega) according to the manufacturer's instructions. The signal was detected by Centro LB960 (Berthold Technologies). The relative light units were calculated by division of the firefly luciferase signal by the renilla luciferase signal. The statistical analysis between the wild type and each mutant was performed by t test.

MG-63 Stable Pool Growth Assay

MG-63 cells were plated the day before transfection at a density of 2×10^6 cells on a 10 cm plate. Cells were transfected with N-terminal GFP-fused wild-type or mutant MN1 vectors via polyethylenimine "Max" (Polysciences). After 48 h, the cells were trypsinised and collected, and the live cells were re-plated at 1×10^6 cells in each well of a six-well plate in duplicate or triplicate with G418 selection (400 μg/mL in reaction) for 5 days. After cells were washed twice with 1× PBS, they were counted by an automatic cell counter with trypan-blue staining (Bio-Rad). Three independent experiments were performed. Statistical t tests between the wild type and each mutant were performed with R 3.6.1.

Establishment of mCAT-HeLa Cell Lines Stably Expressing FLAG-tagged MN1

The full-length wild type and mutant *MN1* ORF were incorporated into the pQCXIP vector (gift from Dr Takahashi) via the

In-Fusion HD Cloning kit (Takara Bio). Each construct was transfected into Plat-E cells through use of the X-tremeGENE 9 transfection reagent (Roche). After 48 h, the supernatant was collected and added into HeLa S3 cells stably expressing mCAT (mCAT-HeLa cells). After the mCAT-HeLa cells reached confluency, puromycin selection (2 μg/mL in reaction) was started. By limiting dilution methods, we were able to pick up and subculture single colonies. We checked the FLAG-tagged *MN1* expression level by immunoblotting with an HRP-fused anti-FLAG antibody (catalog #A8592, M2; Sigma, 1:800).

Immunoprecipitation of the Nuclear Extract and Immunoblotting

mCAT-HeLa, three clones of the MN1-wild type, and three clones of the MN1 mutant stable cell lines (two clones for p.Gln1279* and one clone for p.Arg1295*) were separately cultured up to either 3 or 6 L in Minimum Essential Medium Eagle (Sigma-Aldrich) with 5% calf serum, 2 g/L $NaHCO_3$, and penicillin-streptomycin (Thermo Fisher) at 37°C with 5% CO_2 concentration. The nuclear fraction was extracted by Dignam methods[14] with slight modification. Benzonase nuclease (Sigma-Aldrich) was also used in samples for immunoblotting. The nuclear extract was incubated with anti-FLAG M2 affinity gel (Sigma) for 30 min at 4°C and was then washed three times with wash buffer A (150 mM NaCl, 40 mM HEPES, 0.1% Triton X-100) and twice with wash buffer B (150 mM NaCl, 40 mM HEPES). The 1× FLAG-peptide was added into the slurry so that the FLAG-MN1 complex would be eluted. The eluted samples were run on 4%–20% polyacrylamide gels (Bio-Rad) and stained with the Silver Stain II Kit (WAKO) according to the manufacturer's instructions. We evaluated PBX1, PKNOX1, RING1, and ZBTB24 by immunoblotting with the following antibodies: rabbit polyclonal anti-PBX1 (catalog #4342, Cell Signaling Technology), rabbit polyclonal anti-PKNOX1 (catalog #10614-1-AP, Proteintech), mouse monoclonal anti-RING1 (clone #8C12F4, Santa Cruz Biotechnology), and rabbit polyclonal anti-ZBTB24 (catalog #27975-1-AP, Proteintech). Protein signals were detected with SuperSignal West Femto Maximum Sensitivity Substrate (Thermo Fisher) by the ChemiDoc Touch Imaging System (Bio-Rad).

Protein Identification

The FLAG-tag pulled-down samples were denatured with 2 M urea and 50 mM NH_4HCO_3 and subsequently digested with trypsin for 16 h at 37°C after reduction and alkylation. The resulting peptides were desalted with C18 Stage Tips[15] and were subjected to liquid chromatography tandem-mass spectrometry (LC-MS/MS) analysis. LC-MS/MS analysis was performed on a Triple TOF 5600 (AB SCIEX) coupled with an UltiMate 3000 LC system (Thermo Fisher Scientific). To identify peptides, we created peak lists by using Protein Pilot software v. 5.0.1 (AB SCIEX) and searched against the human protein sequences in the Swiss-Prot database (July 2014) by using the Mascot search engine (v. 2.5.1, Matrix Science) with the following parameters. Enzyme: trypsin. Maximum missed cleavage sites: 2. Variable modifications: N-terminal carbamylation, protein-N-terminal acetylation, carbamidomethylation of cysteine, and oxidation of methionine. Peptide mass tolerance: ± 0.05 Da. Fragment mass tolerance: ± 0.1 Da. We used a 1% overall false-discovery rate as a cutoff to export results from the analysis by MASCOT. In addition, peptides that yielded a peptide ion score >30 were considered positive identifications.

Results

Clinical Features

All three affected individuals were born to healthy nonconsanguineous parents. The common clinical features of these affected individuals include severe developmental delay, speech impairment, characteristic facial features (dolichocephaly, a flat face, thick eyebrows, widely spaced eyes, low-set ears, a short nose, and anteverted nares), and hyperphagia (Figure 1 and Table 1). Serial pictures of individual 3 at different ages suggest that the facial characteristics became more prominent and her face became longer as she grew older (Figures 1C–1H). Although we were unable to show the face of individual 1, his face is similar to those of individuals 2 and 3. His thick and arched eyebrows, anteverted nares, large ear lobes, and rotated ears, in particular, are strikingly similar to those of individual 3. Two of the three affected individuals showed perisylvian polymicrogyria (Figures 1I and 1J). In addition, a high-intensity circular lesion was observed at the left cerebellar white matter on a T2-weighted MRI in individual 3 at the age of 10 years (Figure 1K). However, this finding was not observed in individual 1 at the age of 6 years or individual 2 at the age of 20 months. Therefore, further data collection from affected individuals and longitudinal follow-up would be needed if we are to determine whether this finding is a fundamental feature. See the Supplemental Note for detailed clinical information.

Genetic Analysis

Because all three affected individuals were simplex cases with no family history of consanguinity, we first hypothesized that their condition might be caused by a *de novo* mutation. By trio-based WES, we identified three *de novo* truncating *MN1* variants: c.3883C>T (p.Arg1295*) in individual 1, c.3835C>T (p.Gln1279*) in individual 2, and c.3846_3849del (p.Val1283Thrfs*36) in individual 3 (Figure 2A, Table 1, Table S1). These variants were not registered in any publicly available variant database (gnomAD, ExAC, or EVS) or in our in-house exome control database (n = 575). Interestingly, all three variants were specifically located in exon 2 (Figure 2B). According to the rule of nonsense-mediated mRNA decay (NMD), a premature termination codon at the last coding exon or ~50–55 nucleotides upstream of the last exon–exon junction would escape NMD.[16] Because *MN1* consists of two coding exons, all three variants are thought to escape NMD and produce truncated proteins. Using a lymphoblastoid cell line established from individual 1, we confirmed that the variants did escape NMD (Figure S1). Thus, a truncated MN1 lacking the C-terminal part was thought to stably exist in the cells of individual 1. In addition, a *de novo* missense variant of *ACSL4* (GenBank NM_004458.3, c.1186C>T [p.Arg396Cys]) was detected in individual 3; this variant is classified as "likely pathogenic" according to the ACMG guidelines[17] (PS2, *de novo*; PM2, absent from controls). Loss-of-function variants of *ACSL4* are known to cause X-linked dominant intellectual disability

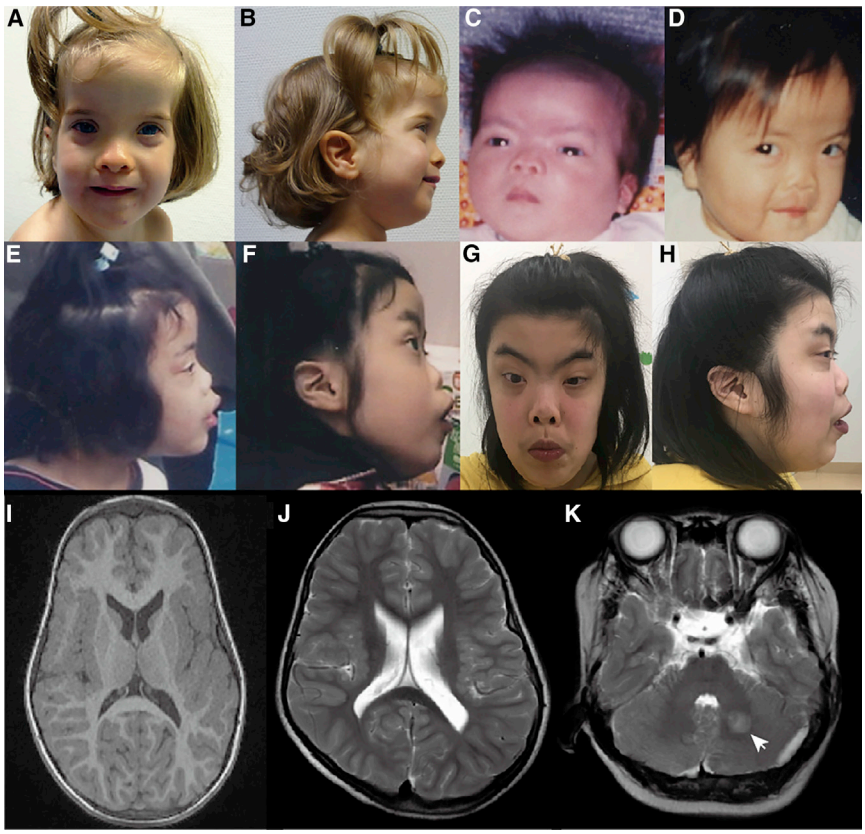

Figure 1. Clinical Features of Two Affected Individuals with Pathogenic *MN1* Variants

(A–H) Facial photographs of affected individuals harboring *de novo MN1* variants. Individual 2 at the age of 2 years old (A and B) and individual 3 at the ages of 1 month old (C), 1 year (D), 6 years (E), 7 years (F), and 18 years old (G and H).

(I) A T1-weighted axial image of brain MRI of individual 2 at the age of 20 months shows polymicrogyria.

(J and K) T2-weighted axial images of individual 3 at 10 years of age. Irregular small gyri that were compatible with polymicrogyria were seen at the bilateral insular cortex (J). The lateral ventricles were mildly dilated, and cavum vergae was observed. A demarcated high-intensity lesion on T2-weighted (K, white arrow) and FLAIR images (data not shown) was observed at the left cerebellar white matter.

(MIM: 300387),[18] but her phenotype, especially the characteristic facial features, cranial anomalies, polymicrogyria, and hyperphagia, cannot be solely explained by the *ACSL4* variant. Therefore, the *MN1* variant is likely to make a significant contribution to the phenotype of individual 3.

MN1 expression has been reported in skeletal muscle in adult humans.[19] In our analysis, *MN1* demonstrated high expression in fetal and adult skeletal muscle and even higher expression in fetal brain (Figure S2).

Intrinsically Disordered Regions in MN1

It has been reported that MN1 contains an N-terminal nuclear localization signal, proline-rich sequences, and two polyglutamine stretches.[19] In addition, one coiled-coil region (518–561 aa) was predicted by the SMART program (Figure S3). PONDR, a web-based prediction software for natural disordered regions, predicted a majority of MN1 to be IDR (Figure 2C), suggesting that the majority of MN1 does not form a fixed tertiary structure. However, all three truncation variants were located within the C-terminal ordered region (from Ser1276 to Thr1320) (Figure 2B, Figure S4). Because all three mutations result in the lack of the C-terminal ordered region (Figure 2D), the three variants raise the IDR fraction of MN1.

Next, we considered the protein sequences of the IDRs of MN1 to speculate about the effect of the IDR on MN1 function. Two types of IDR have been reported: one type is a prion-like IDR composed of mostly polar amino acids, such as serine, tyrosine, glutamine, asparagine, and glycine, which can form aggregates because of their insolubility in water and increased multivalent interactions, whereas the other type is composed of positively- or negatively-charged amino acids undergoing electrostatic interactions.[20] The protein sequence of the low-complexity region or IDR of MN1 is likely to be a prion-like IDR (Figure S5).

Pathogenic MN1 Variants Enhance Aggregation in HeLa Cells and Increase Protein Stability

To address the functional consequences of the truncated MN1 proteins, we examined the subcellular localization of both the wild-type and truncated proteins by transient expression in HeLa cells. As previously reported, GFP-fused wild-type MN1 was localized to the nucleus (Figure S6). Some portion of the cells showed an aggregated pattern even in the wild type, implying that MN1 tends to aggregate with increased insolubility and multivalent interactions. Importantly, enhanced aggregation within nuclei was recognized in mutant constructs (Figure 3A). Then, we quantified the number and size of the MN1 aggregates in the nuclei and observed that MN1 mutant proteins tended to form larger aggregates with higher intensity than wild-type MN1 (Figure 3B, Figure S7). Proteins containing a large IDR portion tend to form phase-separated regions in the nucleus,[21] and our results might thus indicate that all three variants increased the fraction of MN1 IDRs associated with phase separation in cells. To address whether the MN1 variant is involved in phase separation, we used 1,6-Hexanediol to disrupt weak hydrophobic interactions in cells in order to detect any alteration of phase separation.[22] After 1,6-hexanediol treatment, the MN1 aggregates diffused over the nucleoplasm and into the cytoplasm

Table 1. Clinical Features of Affected Individuals with *MN1* Mutations

ID	Individual 1	Individual 2	Individual 3
Ethnicity	Japanese	French	Japanese
Gender	male	female	female
MN1 mutation	c.3883C > T	c.3835C > T	c.3846_3849del
Protein alteration	p.Arg1295*	p.Gln1279*	p.Val1283Thrfs*36
Age at last examination	6 years, 3 months	4 years, 8 months	18 years, 10 months
Height (SD)	102.5 cm (−2 SD)	100 cm (−1 SD)	151.2 cm (−1.3 SD)
Weight (SD)	15.1 kg (−1.8 SD)	15.7 kg (mean)	50.4 kg (−0.3 SD)
Head circumference (SD)	50.7 cm (−0.2 SD)	54 cm (+3 SD)	56.0 cm
Developmental delay	severe	severe	severe
Speech impairment	+	+	+
Epilepsy	−[a]	−	−
Cranial anomaly	dolichocephaly	dolichocephaly	platystencephaly
Characteristic face	+	+	+
Prominent forehead	+	+	−
Flat face	+	+	+
Thick eyebrow	+	+	+
High, arched eyebrow	+	−	+
Widely spaced eyes	+	+	+
Posteriorly rotated ears	+	−	+
Low-set ears	+	+	+
Depressed nasal bridge	+	−	+
Depressed nasal ridge	+	±	+
Short nose	+	+	+
Anteverted nares	+	+	+
Cleft palate	− (narrow palate)	−	− (high arched palate)
Hypotonia	−	+	+
Feeding difficulty	+	+	−
Hyperphagia	+	+	+
Brain images	normal at 6 years, 4 months	polymicrogyria, vermis dysplasia	polymicrogyria

[a]Febrile convulsion three times.

(Figure 3C, Figure S8). Removal of 1,6-hexanediol recovered MN1 aggregate formation not only in the nucleus but also in the cytoplasm, and MN1 aggregates were re-enriched in nuclei within 30 min. These results suggest that accumulated MN1 forms liquid droplet-like protein condensates.

MN1 Protein Stability and Ubiquitin-Proteasome-Pathway-Dependent Degradation

To test the protein levels of wild-type and mutant MN1 in cells, we performed immunoblotting of MN1 transiently overexpressed in cells. We found that mutant MN1 protein accumulated more than wild-type MN1, although the same amount of plasmid encoding wild-type or mutant MN1 was transfected into cells (Figures 4A and 4B). Next, we confirmed similar levels of wild-type and mutant *MN1* transcripts in HEK293T cells transiently expressing *MN1* (Figure S9 and Table S2). These results suggested the possibility that the *MN1* pathogenic variants found in this study might affect the protein stability in cells. To address this question, we examined MN1 stability after CHX treatment by using HEK 293T cells overexpressing wild-type or mutant MN1. We found that the wild-type MN1 was rapidly reduced after CHX treatment, and the reduction of its protein level was abolished by MG132, a proteasome inhibitor,[23] suggesting that MN1 protein is degraded through the ubiquitin–proteasome pathway (Figures 4C and 4D). We also found that MN1 mutants showed more protein stability than the wild type. These results suggest that the

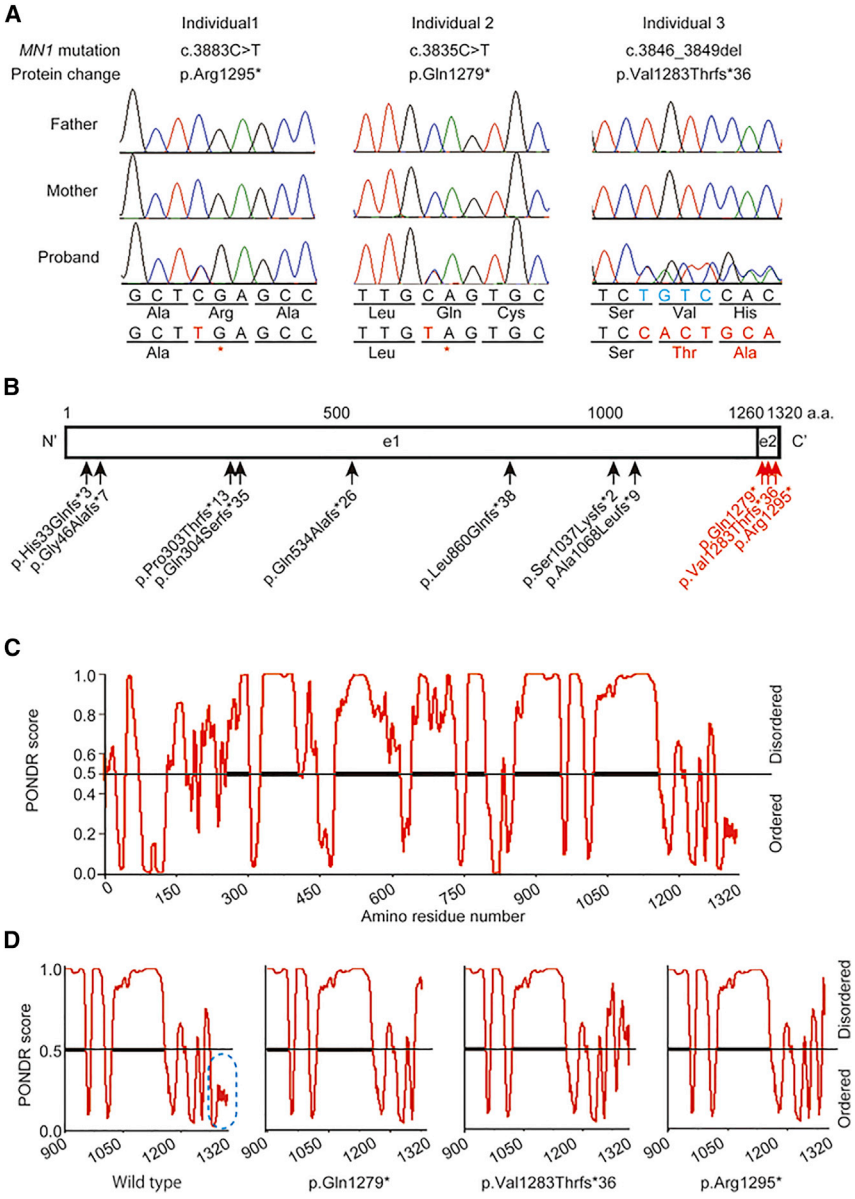

Figure 2. *MN1* Variants and Predicted Ordered and Disordered Regions of MN1

(A) Electropherograms of the three affected individuals with *de novo MN1* truncation variants. The altered nucleotides and amino acid residues are shown in red, and the four deleted base pairs in individual 3 are shown in light blue.

(B) Protein structures of wild-type MN1 and the MN1 loss-of-function variants. The variants registered in gnomAD and identified in affected individuals of this study are shown in black and red, respectively. e1 and e2 are the region encoded by exon1 and exon2.

(C) MN1 disordered and ordered regions predicted by PONDR.

(D) PONDR-predicted mutational effects on the C-terminal ordered region (blue oval with dotted line). The results shown for each are for the C-terminal region (900–terminal codon).

C-terminal region of MN1 is required for degradation through the ubiquitin-proteasome pathway, and its variants interfere with degradation of mutant MN1; this interference leads to increased aggregation of mutant MN1.

Intrinsic Transactivation Activity of MN1

We measured the transactivation activity in wild-type MN1 and the three mutants with a luciferase assay. The wild-type MN1 showed substantial transactivation, as previously reported,[1] and all three mutants showed transactivation activity (Figure 4E). This result is supported by the fact that the mutants maintain the region critical for transactivation activity.

Inhibitory Effect of MN1 on Cell Growth

Because MN1 induction leads to cell-growth inhibition in MG63 cells,[24] we examined whether cell proliferation would be more strongly suppressed in mutants than it would be in wild type. Cell proliferation was more strongly inhibited in cells transfected with the mutant protein than it was in wild-type cells (Figure 4F). The enhanced protein stability, retained transactivation activity, and stronger inhibitory effect on cell proliferation might together indicate that the mutants have a "gain-of-function" effect.

Identification of MN1 Binding-Partner Proteins

Several proteins, including TBX22, MEIS1, MEIS2, HOXA9, HOXA10, and KAT8, have been suggested to be functionally related to MN1. In mice, upregulated *Mn1* expression was reported to increase *Tbx22* expression.[9] KAT8 is recruited to the *MN1* promoter, and its knockdown increases MN1 levels.[25] MEIS1, a transcriptional regulator, shares similar promoter binding sites with MN1.[26] In addition, the N-terminal region of MN1 is important for proliferation and leukemogenesis via upregulation of *HoxA9*, *HoxA10*, and *Meis2*.[27] However, no direct interactions of these six molecules with MN1 have been proven experimentally. To our knowledge, only EP300 and RAC3 have been reported to bind to MN1 in Hep3B cells.[4] Despite this, we saw no evidence of binding between MN1 and RAC3 after immunoprecipitation with the soluble fraction when we transiently co-expressed both proteins in HEK293T cells (data not shown). Because MN1 does not contain a DNA-binding domain, and MN1 itself has transactivation activity, MN1 possibly activates transcription by binding to other DNA-binding transcription factors that can bind enhancer and/or promoter regions.[4] To determine the MN1

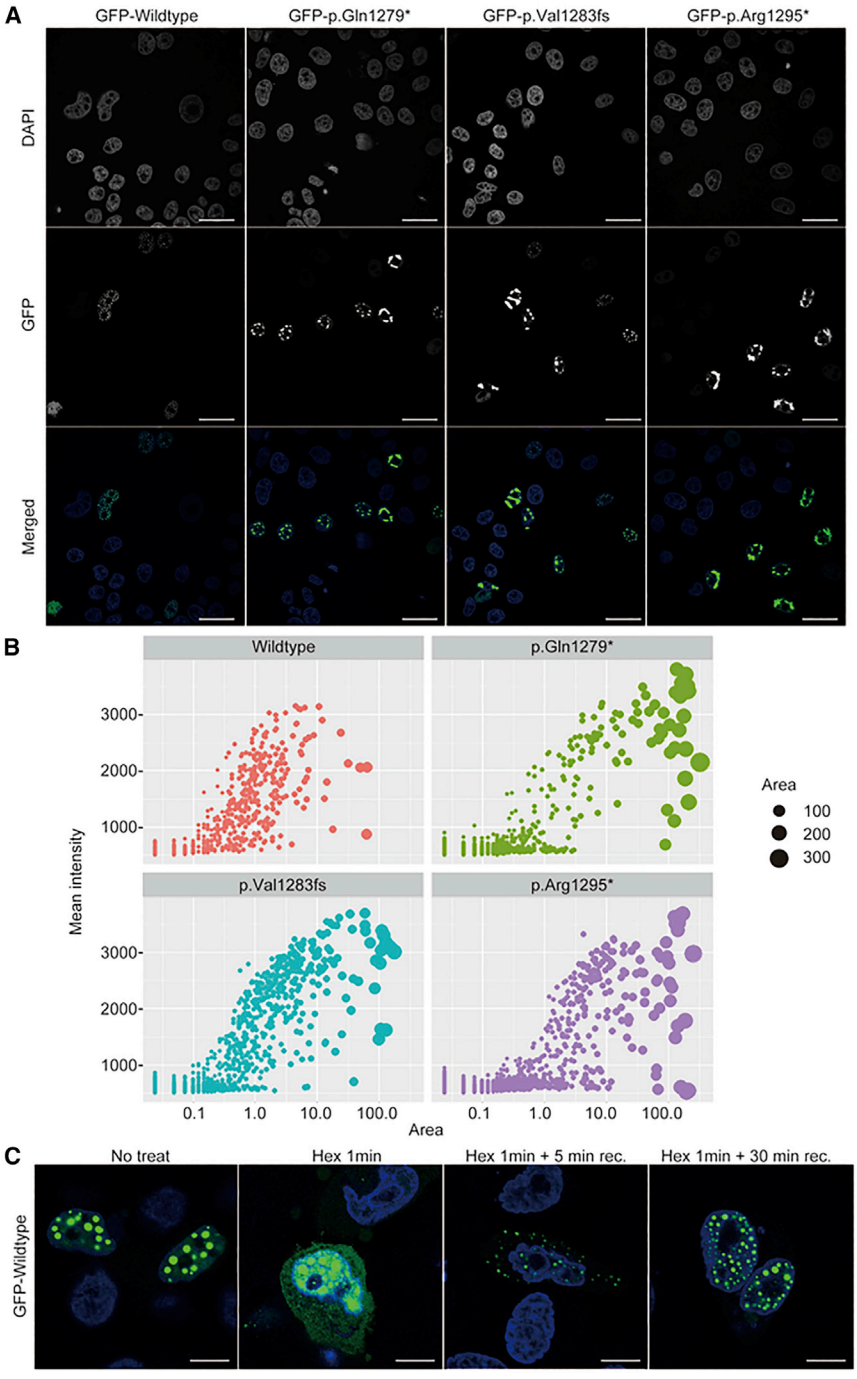

Figure 3. MN1 Subcellular Localization and Protein Aggregation

(A) Immunofluorescence of GFP-fused MN1 proteins. Scale bars represent 20 μm.
(B) Quantification of MN1 aggregates in HeLa cells. The horizontal and vertical axes indicate the aggregation area and mean intensity of each aggregates, respectively.
(C) The effect of 5% 1,6-hexanediol (Hex) treatment of the cells on MN1 aggregation. Scale bars represent 10 μm.

transcriptional regulatory machinery, we looked for transcription factors that bind MN1. We prepared nuclear extracts from mCAT-HeLa cells stably expressing FLAG-tagged MN1 wild-type and mutant proteins (c.3883C>T [p.Arg1295*]) and performed immunoprecipitation and subsequent mass spectrometry analysis (Tables S3–S5). Seven proteins were commonly found in wild-type and mutant cells (Table 2, Figures S10 and S11). Among them, PBX1, PKNOX1 (formerly PREP1), and ZBTB24 are transcription factors. Notably, PBX1 and PKNOX1 function as a heterodimer and play a critical role in development.[28] Through gel-based mass-spectrometric analysis, we confirmed that both MN1 wild-type and mutant proteins copurified with PBX1 (Figure 5A). Furthermore, we also confirmed, through immunoprecipitation, that MN1 binds PBX1 and PKNOX1 (Figure 5B). These results suggest that MN1 plays a role in transcriptional regulation through interaction with the DNA-binding transcription factors PBX1 and PKNOX1. Additionally, our mass spectrometry and/or band-specific proteome analyses revealed that wild-type MN1 copurified with KIF11, RING1, E2F7, and ZBTB24, and mutant MN1 copurified with MEIS1 and PBX2 (Table 2, Figure 5A), suggesting that multiple proteins, including PBX1 and PKNOX1, are also involved in transcriptional regulation with MN1. In addition, we confirmed via immunoblotting that MN1 binds transcription factor ZBTB24 and E3 ubiquitin ligase RING1 (Figure 5B). Mutant MN1 displayed impaired interaction with ZBTB24 and no binding to RING1.

Transcriptome Analysis in Lymphoblastoid Cells from an Affected Individual

To assess the effects of the mutant MN1 protein on transcriptional regulation, we performed RNA-Seq analysis by using lymphoblastoid cells established from individual 1. When we compared this with RNA-Seq data from two unrelated normal controls and one individual affected with leukoencephalopathy with brain-stem and spinal-cord involvement and lactate elevation (MIM: 611105) (as a disease control), we found many upregulated and downregulated genes (Tables S6 and S7). *RAMP1*, *ANKRD18A*, and *VAMP7* were highly ranked in the upregulated genes, and *RRSS21*, *PITX1*, and *ITGB5* were markedly downregulated.We also found some upregulated genes that are associated with neuronal development: *LSAMP* (formerly *LAMP*), which plays an important role

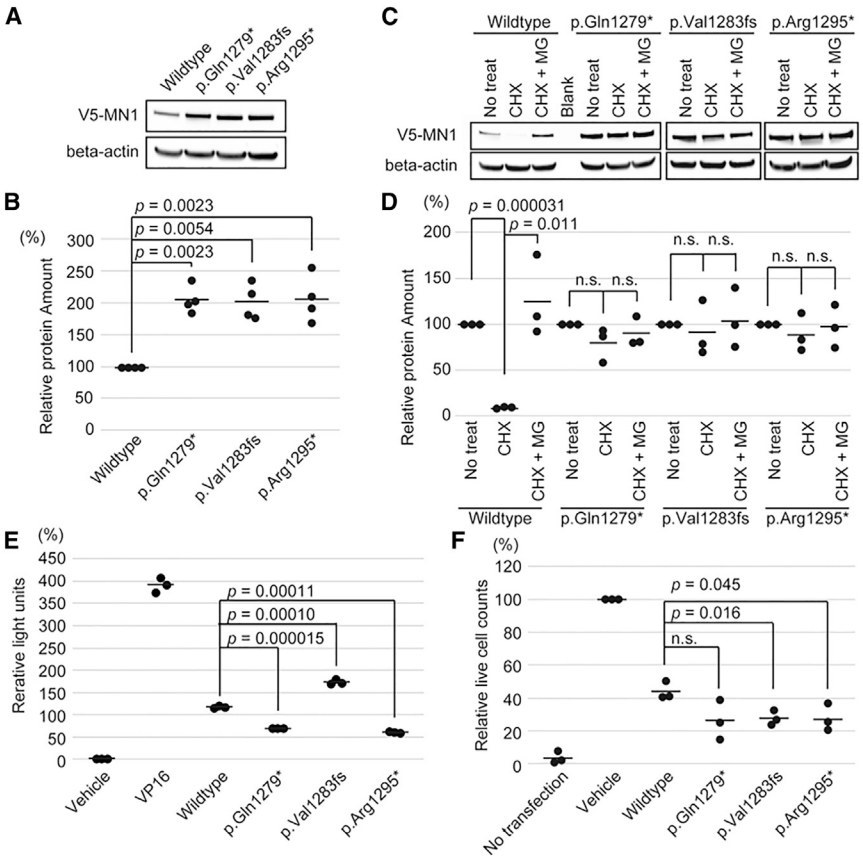

Figure 4. Protein Stability, Transactivation Activity, and Cell proliferation Inhibitory Effect of MN1

(A and B) Immunoblot and quantification of HEK293T cells transiently overexpressing V5-tagged wild-type and mutant MN1 (136 kDa). The amount of MN1 was normalized by β-actin (42 kDa). The wild-type protein amount is set as 100%. Four independent experiments were performed, and comparisons between the wild type and each mutant were analyzed by Welch's test.

(C and D) Immunoblot and quantification of HEK 293T cells transiently overexpressing V5-tagged wild-type and mutant MN1 treated with cycloheximide (CHX) or with CHX and MG132 (MG) for 6 h. The amounts of V5-tagged MN1 were normalized with β-actin. The amount of MN1 in cells that had received no treatment was set as 100% for each construct's transfection. Statistical analysis was performed by Welch's test between no treatment and CHX and by t test between CHX and CHX with MG132.

(E) Dual luciferase assay for transiently overexpressed *MN1* in HEK 293T cells. The statistical analysis was performed by t test.

(F) Relative cell counts of MG63 transiently transfected with empty vector (GFP) as a vehicle, GFP-MN1-wild-type, and GFP-MN1 mutant constructs at day 5 after G418 selection. Cell counts of the empty-vector transfection are set as 100%. This experiment was statistically examined by t test. n.s.: not statistically significant. The bars indicate the mean.

in post-mitotic neuron development, [29,30] and *ITGA*, which encodes integrin alpha-1, which forms a heterodimer with integrin beta-1 and functions in neurite outgrowth.[31,32] In addition, some upregulated genes, such as *SSH3*, are linked to the regulation of the actin cytoskeleton. *SSH3*, one member of the SSH protein family (SSH1, SSH2, and SSH3), plays a role in actin dynamics by reactivating ADF/cofilin[33] (Table S6 and Figure S12).

Next, we performed gene-ontology analysis. When we set the threshold p value at <0.01 and false-discovery rate (FDR) at <1 (Tables S8 and S9), we found gene enrichment in "cell surface" (p value = 0.0005, FDR = 0.644) for upregulated genes and in "positive regulation of ERK1 and ERK2 cascade" (p value = 0.00033, FDR = 0.497), "cell junction" (p value = 0.00061, FDR = 0.749), and "signal peptide" (p value = 0.00042, FDR = 0.605) for the downregulated genes; this enrichment was possibly linked to the phenotype.

Discussion

Here, we reported on three individuals harboring *MN1* truncation variants clustered in exon 2. The three truncation variants identified in our individuals were located within exon 2, whereas other truncation variants that were identified in normal controls and registered in gnomAD are located in exon 1, which might be subject to NMD (Figure 2B). The most common loss-of-function *MN1* variant (chr22, g.28194932_2819493insC [c.1599_1600insG] [p.Gln534Alafs*26]) (Figure 2B) registered in gnomAD was observed in 32 alleles of 9,254 control African individuals (18,508 alleles). Because there are no homozygous individuals, the estimated rate of heterozygous carriers of this loss-of-function variant would be 3.4 out of 1,000 healthy control individuals. Because this frequency might be too high for heterozygosity to be pathogenic, it was thought that heterozygous loss of *MN1* might lead to nophenotype or to only a very mild phenotype. In addition, the haploinsufficiency score of *MN1* is 39.08% (where 0%–10% indicates haploinsufficiency)[34] according to the Decipher database. These reports suggest that the *MN1* variants identified in our affected individuals would be gain-of-function or dominant-negative mutations rather than loss-of-function mutations. In addition, the stronger inhibition of cell growth in mutants than in the wild type indicates a gain of function. An *MN1* missense variant was reported in an individual with nonsyndromic cleft palate only (nsCPO).[10] However, the three individuals with *MN1* truncation mutations reported herein did not show any evidence of a cleft palate, which indicates that the pathomechanism

Table 2. List of Candidate Binding Partners of MN1

Category	Gene Symbol	Uniprot ID	Protein Description
Commonly detected in wild type and mutant	*DDX39A*	O00148	ATP-dependent RNA helicase DDX39A
	TPM3	P06753	tropomyosin alpha-3 chain
	PBX1	P40424	pre-B cell leukemia transcription factor 1
	PKNOX1	P55347	homeobox protein PKNOX1
	PRKDC	P78527	DNA-dependent protein kinase catalytic subunit
	EEF1A1P5	Q5VTE0	putative elongation factor 1-alpha-like 3
	TNPO1	Q92973	transportin-1
Detected only in wild type	*ZBTB24*	O43167	zinc-finger- and BTB-domain-containing protein 24
	PRC1	O43663	protein regulator of cytokinesis 1
	TOP2A	P11388	DNA topoisomerase 2-alpha
	KRT10	P13645	keratin. type I cytoskeletal 10
	KIF11	P52732	kinesin-like protein KIF11
	RING1	Q06587	E3 ubiquitin-protein ligase RING1
	EIF4A2	Q14240	eukaryotic initiation factor 4A-II
	SMU1	Q2TAY7	WD40 repeat-containing protein SMU1
	MOB2	Q70IA6	MOB kinase activator 2
	E2F7	Q96AV8	transcription factor E2F7
	SPIN2B	Q9BPZ2	spindlin-2B
	PNN	Q9H307	pinin
	KCTD5	Q9NXV2	BTB/POZ-domain-containing protein KCTD5
	ANAPC7	Q9UJX3	anaphase-promoting complex subunit 7
Detected only in mutant	*MEIS1*	O00470	homeobox protein Meis1
	RSL1D1	O76021	ribosomal L1-domain-containing protein 1
	BAG2	O95816	BAG family molecular chaperone regulator 2
	ACTN1	P12814	α-actinin-1
	ATF1	P18846	cyclic AMP-dependent transcription factor ATF-1
	PCMT1	P22061	protein-L-isoaspartate (D-aspartate) O-methyltransferase
	PAICS	P22234	multifunctional protein ADE2
	PBX2	P40425	pre-B cell leukemia transcription factor 2
	MSH2	P43246	DNA mismatch repair protein Msh2
	FMR1	Q06787	fragile X mental retardation protein 1
	HDAC1	Q13547	histone deacetylase 1
	CCAR2	Q8N163	cell cycle and apoptosis regulator protein 2
	TXNDC5	Q8NBS9	thioredoxin domain-containing protein 5
	DPY30	Q9C005	protein dpy-30 homolog

of the *MN1* variants we found might differ from that of nsCPO. Of the three variants in this study, one nonsense variant (c.3883C>T [p.Arg1295*]) was reported in two individuals registered in denovo-db. One individual showed developmental delay (DDD4K.03983), and the other showed unclassified generalized epilepsy (Helbig120).[35] Therefore, c.3883C>T is a recurrent *de novo* variant (mutation hotspot).

We showed that the variant c.3883C>T (p.Arg1295*) escaped from NMD (Figure S1) and that proteins lacking the C terminus are more stable than the wild type (Figures 4A–4D). Thus, the C-terminal ordered region is critical for protein degradation. It is possible that this ordered region could be recognized by proteins related to protein degradation. Interestingly, RING1 was only copurified with wild-type MN1, not

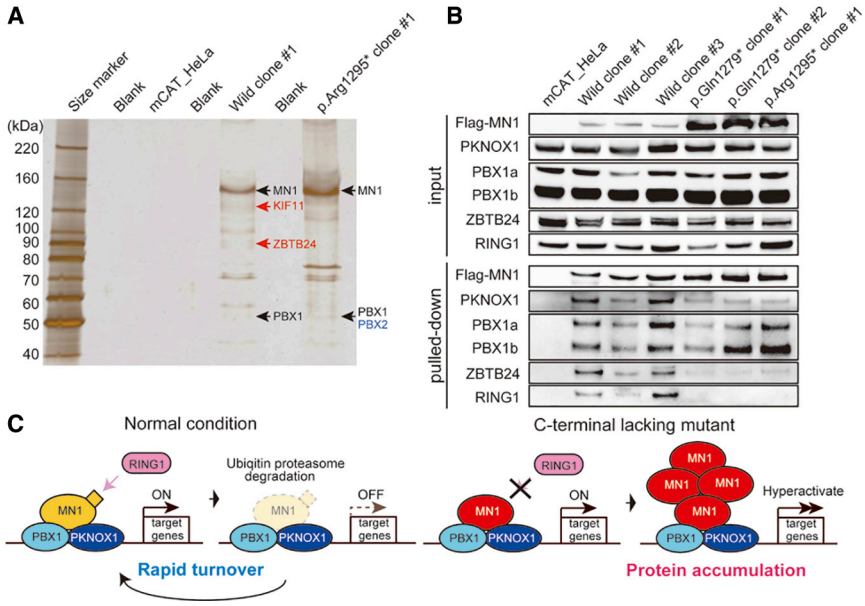

Figure 5. Binding Partners of Wild-Type and Mutant MN1 and Predicted Pathomechanism of *MN1* Truncation Variants

(A) Silver stain of FLAG-immunoprecipitated samples and identified proteins by band-specific proteome analysis.

(B) Immunoblot of anti-FLAG immunoprecipitates from the nuclear extracts of three clones of mCAT-HeLa cells expressing wild-type MN1 and three clones of mCAT-HeLa cells expressing mutant MN1 (two different clones for p.Gln1279* and one clone for p.Arg1295*).

(C) The pathomechanism predicted to result from C-terminally defective MN1 for this specifically recognizable syndrome.

mutant MN1, in our mass-spectrometry (Table 2) and immunoblotting experiments (Figure 5B). RING1 is an E3 ubiquitin ligase, which directly binds and triggers the degradation of p53 through ubiquitination.[36] Thus, MN1 degradation via ubiquitination by RING1 might be abrogated in the mutant MN1 lacking the C-terminal ordered region, and this abrogation might lead to mutant MN1 enrichment and dysregulation of MN1-related transcription (Figure 5C). Proper degradation of MN1 might contribute to precise transcriptional regulation via the appropriate turnover of MN1 protein.

By mass spectrometry and immunoblotting, we identified PBX1 and PKNOX1 as MN1-binding transcription factors in stable cell lines expressing wild-type and mutant MN1, and we identified MEIS1 in a stable cell line expressing mutant MN1. PKNOX1 (tumor-suppressor gene) and MEIS1 (oncogene) competitively bind to PBX1,[37] and they regulate PBX1 protein stability.[38] Furthermore, MEIS1-PBX1 and PKNOX1-PBX1 heterodimers form ternary complexes with anterior Hox proteins and thus modulate the specificity of Hox-dependent gene expression.[39–41] Hoxb1 and Hoxb2, with Pknox1 and Pbx1, also play an important role in hindbrain development.[41,42]

The transcription factors ZBTB24 and E2F7 only bound wild-type MN1 in our mass-spectrometric analysis (Table 2). Notably, *ZBTB24* (MIM: 614064, GenBank: NM_014797.2) abnormalities cause the autosomal-recessive immunodeficiency, centromeric instability, and facial anomalies syndrome 2 (ICF; MIM: 614069).[43] Intellectual disability, a depressed nasal bridge, widely spaced eyes, and low-set ears are commonly seen in this *MN1*-related syndrome. It has been shown that ZBTB24 plays a role in the activation and repression of genes transcription.[44] We also confirmed by immunoblot that ZBTB24 preferentially binds wild-type MN1 (Figure 5B). Thus, our results raise the possibility that MN1 plays a role as a cofactor of ZBTB24 and regulates gene expression in addition to the PBX1-PKNOX1 transcriptional pathway.

A unique feature of MN1 is that the majority of the protein consists of IDRs (Figure 2C, Figures S3–S5). IDRs do not have static structures but have high specificity and low interaction with their functional partners. This is the key property that enables transient interactions between proteins and between proteins and nucleic acids during signal transduction, recognition, and regulation.[45] Because the IDRs of MN1 are prion-like IDRs, MN1 tends to form aggregations via increased insolubility and multivalency even in the normal state, and mutant MN1 showed enhanced aggregation as a result of the lack of the C-terminal ordered region, as shown in Figures 3A and 3B. The other possibility is that the IDRs of MN1 might contribute to phase separation; multivalent interacting proteins consisting of IDRs have been implicated in liquid-liquid phase separation in cells.[46,47] Cellular bodies, membrane-less organelles composed of a high density of protein and nucleic acids, play pivotal roles in eukaryotic cells in compartmentalizing essential biochemical reactions and are formed by phase separation.[48–50] By a similar mechanism, super-enhancers, which are made up of several hundred clusters of enhancers composed of transcription factors, cofactors, chromatin regulators, RNA polymerase II, and noncoding RNA,[51] are thought to form by phase separation.[52] This is especially important for cell identity.[51,53] Condensation in phase separation depends on the number and concentration of the interacting molecules and the number of binding sites.[52] The mutant MN1, with increased protein stability, might lead to a higher concentration of MN1 within a cell. In addition, coactivator condensation regulates phase separation and gene expression in super-enhancers.[21] Thus, mutant MN1 might alter the phase separation and change gene expression in development.

Here we report on a recognizable syndrome characterized by unique craniofacial abnormalities and severe developmental delay. Our experiments strongly indicate that

the truncated *MN1* variants found in this study produce gain-of-function proteins lacking the C terminus. In light of the IDR-enriched structure of MN1, the enhanced aggregation of mutant MN1 in nuclei suggests the involvement of altered phase separation. We also present evidence that MN1 binds to the PBX1-PKNOX1-MEIS1-PBX2 complex, and we list dysregulated genes. Further research is absolutely needed if we are to understand the pathomechanism of the *MN1*-related disease and the role of *MN1* in human development.

Acknowledgments

We thank the affected individuals and their families for participating in this study. The gel-based mass-spectrometric analysis was kindly performed by Mizuho Oda, Emiko Koda, Masaki Matsumoto, and Keiichi Nakayama in the Cooperative Research Project Program of the Medical Institute of Bioregulation, Kyushu University. This work was supported by AMED grants JP19ek0109280, JP19dm0107090, JP19ek0109301, JP19ek0109348, and JP18kk020501 (to N. Matsumoto); JSPS KAKENHI grants JP17H01539 (to N. Matsumoto) and JP19H03621 (to N. Miyake); and grants from the Ministry of Health, Labor, and Welfare (to N. Matsumoto) and the Takeda Science Foundation (to N. Matsumoto and N. Miyake). We thank Catherine Perfect (Cantab), from Edanz Group (https://www.edanzediting.com/ac), for editing a draft of this manuscript.

Declaration of Interests

The authors declare no competing interests.

Received: July 17, 2019
Accepted: November 15, 2019
Published: December 12, 2019

Supplemental Information

Supplemental Information Data can be found online at https://doi.org/10.1016/j.ajhg.2019.11.011.

Web Resources

denovo-db, http://denovo-db.gs.washington.edu/denovo-db/
Expression Atlas database, https://www.ebi.ac.uk/gxa/home
gnomAD, https://gnomad.broadinstitute.org/
ImageJ, https://imagej.nih.gov/ij/index.html
Online Mendelian Inheritance in Man, https://www.omim.org
PONDR, http://www.pondr.com/
SMART, http://smart.embl-heidelberg.de/
Trim Galore!, http://www.bioinformatics.babraham.ac.uk/projects/trim_galore/
vertebrate genome annotation (VEGA) genes, https://www.bioinformatics.babraham.ac.uk/projects/seqmonk/

References

1. Lekanne Deprez, R.H., Groen, N.A., van Biezen, N.A., Hagemeijer, A., van Drunen, E., Koper, J.W., Avezaat, C.J., Bootsma, D., and Zwarthoff, E.C. (1991). A t(4;22) in a meningioma points to the localization of a putative tumor-suppressor gene. Am. J. Hum. Genet. *48*, 783–790.
2. Buijs, A., Sherr, S., van Baal, S., van Bezouw, S., van der Plas, D., Geurts van Kessel, A., Riegman, P., Lekanne Deprez, R., Zwarthoff, E., Hagemeijer, A., et al. (1995). Translocation (12;22) (p13;q11) in myeloproliferative disorders results in fusion of the ETS-like TEL gene on 12p13 to the MN1 gene on 22q11. Oncogene *10*, 1511–1519.
3. Heuser, M., Beutel, G., Krauter, J., Döhner, K., von Neuhoff, N., Schlegelberger, B., and Ganser, A. (2006). High meningioma 1 (MN1) expression as a predictor for poor outcome in acute myeloid leukemia with normal cytogenetics. Blood *108*, 3898–3905.
4. van Wely, K.H., Molijn, A.C., Buijs, A., Meester-Smoor, M.A., Aarnoudse, A.J., Hellemons, A., den Besten, P., Grosveld, G.C., and Zwarthoff, E.C. (2003). The MN1 oncoprotein synergizes with coactivators RAC3 and p300 in RAR-RXR-mediated transcription. Oncogene *22*, 699–709.
5. Mangelsdorf, D.J., Umesono, K., Kliewer, S.A., Borgmeyer, U., Ong, E.S., and Evans, R.M. (1991). A direct repeat in the cellular retinol-binding protein type II gene confers differential regulation by RXR and RAR. Cell *66*, 555–561.
6. Nakshatri, H., and Bhat-Nakshatri, P. (1998). Multiple parameters determine the specificity of transcriptional response by nuclear receptors HNF-4, ARP-1, PPAR, RAR and RXR through common response elements. Nucleic Acids Res. *26*, 2491–2499.
7. Breckpot, J., Anderlid, B.M., Alanay, Y., Blyth, M., Brahimi, A., Duban-Bedu, B., Gozé, O., Firth, H., Yakicier, M.C., Hens, G., et al. (2016). Chromosome 22q12.1 microdeletions: confirmation of the MN1 gene as a candidate gene for cleft palate. Eur. J. Hum. Genet. *24*, 51–58.
8. Hoebel, A.K., Drichel, D., van de Vorst, M., Böhmer, A.C., Sivalingam, S., Ishorst, N., Klamt, J., Gölz, L., Alblas, M., Maaser, A., et al. (2017). Candidate genes for nonsyndromic cleft palate detected by exome sequencing. J. Dent. Res. *96*, 1314–1321.
9. Liu, W., Lan, Y., Pauws, E., Meester-Smoor, M.A., Stanier, P., Zwarthoff, E.C., and Jiang, R. (2008). The Mn1 transcription factor acts upstream of Tbx22 and preferentially regulates posterior palate growth in mice. Development *135*, 3959–3968.
10. Meester-Smoor, M.A., Vermeij, M., van Helmond, M.J., Molijn, A.C., van Wely, K.H., Hekman, A.C., Vermey-Keers, C., Riegman, P.H., and Zwarthoff, E.C. (2005). Targeted disruption of the Mn1 oncogene results in severe defects in development of membranous bones of the cranial skeleton. Mol. Cell. Biol. *25*, 4229–4236.
11. Said, E., Cuschieri, A., Vermeesch, J., and Fryns, J.P. (2011). Toriello-Carey syndrome with a 6Mb interstitial deletion at 22q12 detected by array CGH. Am. J. Med. Genet. A. *155A*, 1390–1392.
12. Davidson, T.B., Sanchez-Lara, P.A., Randolph, L.M., Krieger, M.D., Wu, S.Q., Panigrahy, A., Shimada, H., and Erdreich-Epstein, A. (2012). Microdeletion del(22)(q12.2) encompassing the facial development-associated gene, MN1 (meningioma 1) in a child with Pierre-Robin sequence (including cleft palate) and neurofibromatosis 2 (NF2): A case report and review of the literature. BMC Med. Genet. *13*, 19.
13. Miyake, N., Tsukaguchi, H., Koshimizu, E., Shono, A., Matsunaga, S., Shiina, M., Mimura, Y., Imamura, S., Hirose, T., Okudela, K., et al. (2015). Biallelic mutations in nuclear pore complex subunit NUP107 cause early-childhood-onset steroid-resistant nephrotic syndrome. Am. J. Hum. Genet. *97*, 555–566.

14. Dignam, J.D., Lebovitz, R.M., and Roeder, R.G. (1983). Accurate transcription initiation by RNA polymerase II in a soluble extract from isolated mammalian nuclei. Nucleic Acids Res. *11*, 1475–1489.
15. Rappsilber, J., Mann, M., and Ishihama, Y. (2007). Protocol for micro-purification, enrichment, pre-fractionation and storage of peptides for proteomics using StageTips. Nat. Protoc. *2*, 1896–1906.
16. Nagy, E., and Maquat, L.E. (1998). A rule for termination-codon position within intron-containing genes: When nonsense affects RNA abundance. Trends Biochem. Sci. *23*, 198–199.
17. Richards, S., Aziz, N., Bale, S., Bick, D., Das, S., Gastier-Foster, J., Grody, W.W., Hegde, M., Lyon, E., Spector, E., et al.; ACMG Laboratory Quality Assurance Committee (2015). Standards and guidelines for the interpretation of sequence variants: A joint consensus recommendation of the American College of Medical Genetics and Genomics and the Association for Molecular Pathology. Genet. Med. *17*, 405–424.
18. Meloni, I., Muscettola, M., Raynaud, M., Longo, I., Bruttini, M., Moizard, M.P., Gomot, M., Chelly, J., des Portes, V., Fryns, J.P., et al. (2002). FACL4, encoding fatty acid-CoA ligase 4, is mutated in nonspecific X-linked mental retardation. Nat. Genet. *30*, 436–440.
19. Lekanne Deprez, R.H., Riegman, P.H., Groen, N.A., Warringa, U.L., van Biezen, N.A., Molijn, A.C., Bootsma, D., de Jong, P.J., Menon, A.G., Kley, N.A., et al. (1995). Cloning and characterization of MN1, a gene from chromosome 22q11, which is disrupted by a balanced translocation in a meningioma. Oncogene *10*, 1521–1528.
20. Alberti, S. (2017). Phase separation in biology. Curr. Biol. *27*, R1097–R1102.
21. Sabari, B.R., Dall'Agnese, A., Boija, A., Klein, I.A., Coffey, E.L., Shrinivas, K., Abraham, B.J., Hannett, N.M., Zamudio, A.V., Manteiga, J.C., et al. (2018). Coactivator condensation at super-enhancers links phase separation and gene control. Science *361*, 361.
22. Strom, A.R., Emelyanov, A.V., Mir, M., Fyodorov, D.V., Darzacq, X., and Karpen, G.H. (2017). Phase separation drives heterochromatin domain formation. Nature *547*, 241–245.
23. Coux, O., Tanaka, K., and Goldberg, A.L. (1996). Structure and functions of the 20S and 26S proteasomes. Annu. Rev. Biochem. *65*, 801–847.
24. Sutton, A.L., Zhang, X., Ellison, T.I., and Macdonald, P.N. (2005). The 1,25(OH)2D3-regulated transcription factor MN1 stimulates vitamin D receptor-mediated transcription and inhibits osteoblastic cell proliferation. Mol. Endocrinol. *19*, 2234–2244.
25. Zhao, W.B., Wang, M., Gao, S., Shaikh, A.S., Chen, J., and Li, X.Z. (2018). The histone acetyltranseferase KAT8 regulates cell differentiation by suppression of MN1 in AML. Br. J. Haematol. *182*, 276–279.
26. Heuser, M., Yun, H., Berg, T., Yung, E., Argiropoulos, B., Kuchenbauer, F., Park, G., Hamwi, I., Palmqvist, L., Lai, C.K., et al. (2011). Cell of origin in AML: Susceptibility to MN1-induced transformation is regulated by the MEIS1/AbdB-like HOX protein complex. Cancer Cell *20*, 39–52.
27. Lai, C.K., Moon, Y., Kuchenbauer, F., Starzcynowski, D.T., Argiropoulos, B., Yung, E., Beer, P., Schwarzer, A., Sharma, A., Park, G., et al. (2014). Cell fate decisions in malignant hematopoiesis: Leukemia phenotype is determined by distinct functional domains of the MN1 oncogene. PLoS ONE *9*, e112671.
28. Zucchelli, C., Ferrari, E., Blasi, F., Musco, G., and Bruckmann, C. (2017). New insights into cooperative binding of homeodomain transcription factors PREP1 and PBX1 to DNA. Sci. Rep. *7*, 40665.
29. Pimenta, A.F., Fischer, I., and Levitt, P. (1996). cDNA cloning and structural analysis of the human limbic-system-associated membrane protein (LAMP). Gene *170*, 189–195.
30. Pimenta, A.F., Reinoso, B.S., and Levitt, P. (1996). Expression of the mRNAs encoding the limbic system-associated membrane protein (LAMP): II. Fetal rat brain. J. Comp. Neurol. *375*, 289–302.
31. Tawil, N.J., Houde, M., Blacher, R., Esch, F., Reichardt, L.F., Turner, D.C., and Carbonetto, S. (1990). Alpha 1 beta 1 integrin heterodimer functions as a dual laminin/collagen receptor in neural cells. Biochemistry *29*, 6540–6544.
32. Rossino, P., Gavazzi, I., Timpl, R., Aumailley, M., Abbadini, M., Giancotti, F., Silengo, L., Marchisio, P.C., and Tarone, G. (1990). Nerve growth factor induces increased expression of a laminin-binding integrin in rat pheochromocytoma PC12 cells. Exp. Cell Res. *189*, 100–108.
33. Niwa, R., Nagata-Ohashi, K., Takeichi, M., Mizuno, K., and Uemura, T. (2002). Control of actin reorganization by Slingshot, a family of phosphatases that dephosphorylate ADF/cofilin. Cell *108*, 233–246.
34. Huang, N., Lee, I., Marcotte, E.M., and Hurles, M.E. (2010). Characterising and predicting haploinsufficiency in the human genome. PLoS Genet. *6*, e1001154.
35. Helbig, K.L., Farwell Hagman, K.D., Shinde, D.N., Mroske, C., Powis, Z., Li, S., Tang, S., and Helbig, I. (2016). Diagnostic exome sequencing provides a molecular diagnosis for a significant proportion of patients with epilepsy. Genet. Med. *18*, 898–905.
36. Shen, J., Li, P., Shao, X., Yang, Y., Liu, X., Feng, M., Yu, Q., Hu, R., and Wang, Z. (2018). The E3 ligase RING1 targets p53 for degradation and promotes cancer cell proliferation and survival. Cancer Res. *78*, 359–371.
37. Dardaei, L., Longobardi, E., and Blasi, F. (2014). Prep1 and Meis1 competition for Pbx1 binding regulates protein stability and tumorigenesis. Proc. Natl. Acad. Sci. USA *111*, E896–E905.
38. Longobardi, E., and Blasi, F. (2003). Overexpression of PREP-1 in F9 teratocarcinoma cells leads to a functionally relevant increase of PBX-2 by preventing its degradation. J. Biol. Chem. *278*, 39235–39241.
39. Jacobs, Y., Schnabel, C.A., and Cleary, M.L. (1999). Trimeric association of Hox and TALE homeodomain proteins mediates Hoxb2 hindbrain enhancer activity. Mol. Cell. Biol. *19*, 5134–5142.
40. Ferretti, E., Schulz, H., Talarico, D., Blasi, F., and Berthelsen, J. (1999). The PBX-regulating protein PREP1 is present in different PBX-complexed forms in mouse. Mech. Dev. *83*, 53–64.
41. Ferretti, E., Marshall, H., Pöpperl, H., Maconochie, M., Krumlauf, R., and Blasi, F. (2000). Segmental expression of Hoxb2 in r4 requires two separate sites that integrate cooperative interactions between Prep1, Pbx and Hox proteins. Development *127*, 155–166.
42. Ferretti, E., Cambronero, F., Tümpel, S., Longobardi, E., Wiedemann, L.M., Blasi, F., and Krumlauf, R. (2005). Hoxb1 enhancer and control of rhombomere 4 expression: Complex interplay between PREP1-PBX1-HOXB1 binding sites. Mol. Cell. Biol. *25*, 8541–8552.

43. de Greef, J.C., Wang, J., Balog, J., den Dunnen, J.T., Frants, R.R., Straasheijm, K.R., Aytekin, C., van der Burg, M., Duprez, L., Ferster, A., et al. (2011). Mutations in ZBTB24 are associated with immunodeficiency, centromeric instability, and facial anomalies syndrome type 2. Am. J. Hum. Genet. *88*, 796–804.
44. Thompson, J.J., Kaur, R., Sosa, C.P., Lee, J.H., Kashiwagi, K., Zhou, D., and Robertson, K.D. (2018). ZBTB24 is a transcriptional regulator that coordinates with DNMT3B to control DNA methylation. Nucleic Acids Res. *46*, 10034–10051.
45. Dyson, H.J., and Wright, P.E. (2005). Intrinsically unstructured proteins and their functions. Nat. Rev. Mol. Cell Biol. *6*, 197–208.
46. Li, P., Banjade, S., Cheng, H.C., Kim, S., Chen, B., Guo, L., Llaguno, M., Hollingsworth, J.V., King, D.S., Banani, S.F., et al. (2012). Phase transitions in the assembly of multivalent signalling proteins. Nature *483*, 336–340.
47. Lin, Y., Protter, D.S., Rosen, M.K., and Parker, R. (2015). Formation and maturation of phase-separated liquid droplets by RNA-binding proteins. Mol. Cell *60*, 208–219.
48. Brangwynne, C.P., Eckmann, C.R., Courson, D.S., Rybarska, A., Hoege, C., Gharakhani, J., Jülicher, F., and Hyman, A.A. (2009). Germline P granules are liquid droplets that localize by controlled dissolution/condensation. Science *324*, 1729–1732.
49. Banjade, S., Wu, Q., Mittal, A., Peeples, W.B., Pappu, R.V., and Rosen, M.K. (2015). Conserved interdomain linker promotes phase separation of the multivalent adaptor protein Nck. Proc. Natl. Acad. Sci. USA *112*, E6426–E6435.
50. Banani, S.F., Lee, H.O., Hyman, A.A., and Rosen, M.K. (2017). Biomolecular condensates: Organizers of cellular biochemistry. Nat. Rev. Mol. Cell Biol. *18*, 285–298.
51. Hnisz, D., Abraham, B.J., Lee, T.I., Lau, A., Saint-André, V., Sigova, A.A., Hoke, H.A., and Young, R.A. (2013). Super-enhancers in the control of cell identity and disease. Cell *155*, 934–947.
52. Hnisz, D., Shrinivas, K., Young, R.A., Chakraborty, A.K., and Sharp, P.A. (2017). A phase separation model for transcriptional control. Cell *169*, 13–23.
53. Whyte, W.A., Orlando, D.A., Hnisz, D., Abraham, B.J., Lin, C.Y., Kagey, M.H., Rahl, P.B., Lee, T.I., and Young, R.A. (2013). Master transcription factors and mediator establish super-enhancers at key cell identity genes. Cell *153*, 307–319.